Internally driven variability of the Angola Low is the main source of uncertainty for the future changes in southern African precipitation

Article

Published Version

It is advisable to refer to the publisher's version if you intend to cite from the work. See Guidance on citing.

Internally Driven Variability of the Angola Low is the Main Source of Uncertainty for the Future Changes in Southern African Precipitation

Paul-Arthur Monerie[1] ![ORCID], **Bastien Dieppois**[2], **Benjamin Pohl**[3] ![ORCID], **and Julien Crétat**[3] ![ORCID]

[1]National Centre for Atmospheric Science, Reading, UK, [2]Centre for Agroecology, Water and Resilience, Coventry University, Coventry, UK, [3]Centre de Recherches de Climatologie, UMR 6282 Biogéosciences, CNRS/Université de Bourgogne, Dijon, France

Abstract Variations in southern African precipitation have a major impact on local communities, increasing climate-related risks and affecting water and food security, as well as natural ecosystems. However, future changes in southern African precipitation are uncertain, with climate models showing a wide range of responses from near-term projections (2020–2040) to the end of the 21st century (2080–2100). Here, we assess the uncertainty in southern African precipitation change using five Ocean-Atmosphere General Circulation single model initial-condition large ensembles (30–50 ensemble members) and four emissions scenarios. We show that the main source of uncertainty in 21st Century projections of southern African precipitation is the internal climate variability. In addition, we find that differences between ensemble members in simulating future changes in the location of the Angola Low explain a large proportion (∼60%) of the uncertainty in precipitation change. Together, the internal variations in the large-scale circulation over the Pacific Ocean and the Angola Low explain ∼64% of the uncertainty in southern African precipitation change. We suggest that a better understanding of the future evolutions of the southern African precipitation may be achieved by understanding better the model's ability to simulate the Angola Low and its effects on precipitation.

Plain Language Summary The variability of precipitation in southern Africa has a strong impact on local communities, rain-fed agriculture, food security and water demand, hydropower production, lake levels, ecosystems, and wildlife. Above-average rainfall increases the risk of flooding, while below-average rainfall increases the risk of drought. However, future changes in precipitation in southern Africa are poorly understood. Here, we examine the potential sources of uncertainty in southern African precipitation change using five ocean-atmosphere general circulation single-model initial-condition large ensembles and four emissions scenarios. We show that the main source of uncertainty is the simulation of internal climate variability throughout the 21st century. Among potential drivers, we show that the main driver of uncertainty in southern African precipitation change is the future change in the location of the Angola low. A future northward (southward) shift of the Angola Low is associated with a future decrease (increase) in southern African precipitation. We suggest that a better understanding of future changes in southern African precipitation could be achieved by better understanding the impact of internal climate variability on the Angola Low.

1. Introduction

Southern Africa shows a high degree of year-to-year variability in seasonal precipitation amounts (e.g., Dieppois et al., 2016, 2019; Reason et al., 2006; Ullah et al., 2023). Coupled with reliance on rain-fed agriculture and growing water demand, the high variability of rainfall increases climate-related risk for local communities. For example, rainfall variability can lead to extreme conditions, such as the so-called 'Day Zero drought' observed in Cape Town in 2018 (Burls et al., 2019; Pascale et al., 2020; Wolski et al., 2021) and more largely all over southern Africa (Ayugi et al., 2022). Precipitation variability is also associated with reductions in lake levels and hydroelectric production (Conway et al., 2017; Siderius et al., 2018), and large impacts on natural ecosystems and wildlife (Dallas & Rivers-Moore, 2014). Above-average rainfall also leads to a higher risk of flooding, with severe consequences for communities in southern Africa (Li et al., 2016; Tramblay et al., 2022).

Southern African precipitation varies on several timescales in response to internal modes of climate variability. On interannual timescales, for example, rainfall in southern Africa is strongly linked to the El Niño Southern Oscillation (ENSO) (e.g., Crétat et al., 2012; Dieppois et al., 2015, 2016, 2019; Gaughan et al., 2016; Gore

et al., 2020; J Malherbe et al., 2016; Ratna et al., 2013; Ratnam et al., 2014). In addition to ENSO, changes in the strength and location of the Angola Low (AL) modulate the interannual variability of the southern African precipitation (Crétat et al., 2019; Howard et al., 2019; Pascale et al., 2019). On decadal timescales, the effect of ENSO on southern African precipitation is modulated by decadal modes of climate variability in the Pacific Ocean (e.g., Pacific Decadal Oscillation, Interdecadal Pacific Oscillation (Pohl et al., 2018; Dieppois et al., 2016, 2019; J Malherbe et al., 2016; Reason & Rouault, 2002), the Indian Ocean (e.g., subtropical Indian Ocean dipole [SIOD]; Behera & Yamagata, 2001), the Southern Hemisphere large-scale circulation (e.g., Southern Annular Mode), and the Hadley circulation (J. Malherbe et al., 2016, 2014).

Another source of precipitation anomaly is the effect of climate change, which is mostly associated with the effects of anthropogenic activity. The externally forced response is associated with a weak to moderate change in precipitation, with a wetter climate over tropical Africa and a contrasted decline in precipitation further south (Pohl et al., 2017). However, changes in precipitation are uncertain and model-dependent, with a low inter-model agreement in the simulated change in precipitation, particularly during the wet season in the Austral summer (Almazroui et al., 2020; Dosio et al., 2021; Munday & Washington, 2019; Pohl et al., 2017; Wu et al., 2024). Changes appear to be more robust when considering extreme events (Pohl et al., 2017), with climate change increasing the likelihood of a new Day Zero drought (Pascale et al., 2020). In addition to changes in precipitation, climate change is leading to a large increase in potential evapotranspiration and, therefore, a drier climate over southern Africa (Ukkola et al., 2020).

While there is evidence that climate change may strongly affect the southern African climate, through an increase in the frequency and intensity of extreme events, such as heatwaves, heavy rainfall and drought (Pohl et al., 2017; Ukkola et al., 2020), uncertainties in climate change projections for southern Africa remain high. We also know very little about the source of these uncertainties in regional climate change projections. As highlighted by Lehner et al. (2020), near-term changes in southern African precipitation conditions could be strongly uncertain because of: (a) differences in model physics and/or model sensitivity to externally forced changes in global radiative forcing; (b) different sequences of internally driven climate variations; (c) alternative socio-economic and emissions scenarios, as well as different horizons. Improving our understanding of future changes is important for decision-makers and water management, for instance. Understanding both aforementioned sources of uncertainty is thus critical and requires large ensembles of simulations (Deser et al., 2014; Lehner et al., 2020; Maher et al., 2019; Paul-Arthur Monerie et al., 2017). This scientific and societally relevant question has yet to be addressed so far in the literature. We bridge this gap by assessing how internal climate variability could affect the future change in precipitation relative to the externally forced response. In particular, we address the following questions:

- What are the contributions of the three main sources of uncertainty (internal variability, model, and scenario uncertainty) to future changes in southern African precipitation?
- What are the mechanisms at play behind the uncertainty in the change in southern African precipitation?

The paper is organized as follows. Section 2 describes the data and methods. In Section 3, we analyze the effect of both the externally forced response and internal climate variability on southern African precipitation. The results are discussed in Section 4, and Section 5 summarizes the main findings of the study.

2. Data and Method

2.1. Climate Model Simulations

We use five Ocean-Atmosphere General Circulation Single Model Initial-condition Large Ensembles (SMILEs) (Table 1) forced by four future emissions pathways (SSP1-2.6; SSP2-4.5; SSP3-7.0 and SSP5-8.5), for which we have between 30 and 50 ensemble members. All ensemble members of the same model differ from their initial conditions. Multiple SMILEs and emissions scenarios allow us to assess the contribution of the three main sources of uncertainty in southern African precipitation changes. All models participated in the sixth phase of the Coupled Model Intercomparison Project (CMIP6; Eyring et al., 2016).

All data were re-gridded to a common horizontal resolution of $1.5° \times 1.5°$ using bilinear interpolation to facilitate comparison between models. We use monthly means to assess future changes in the southern African climate.

Table 1
Names, Number of the Available Ensemble Members for Each Scenario, Horizontal Resolutions and References of the Five Single Model Initial-Condition Large Ensembles Used in This Study

Model	Number of ensemble members	Res. (Lat × lon)	References
ACCESS-ESM-1-5	40	145 × 192; 1.25° × 1.875°	Ziehn et al. (2020)
CanESM5	50	64 × 128; ~2.79° × 2.81°	Swart et al. (2019)
MIROC6	50	128 × 256; 1.4° × 1.4°	Tatebe et al. (2019)
MPI-ESM1-2-LR	30	96 × 192; ~1.85° × 1.875°	Mauritsen et al. (2019)
Ec-Earth3	50	256 × 512; 0.7° × 0.7	Wyser et al. (2020)

We also compare the SMILEs' results to an ensemble mean composed of the outputs of 42 climate models (Table S1 in Supporting Information S1), using a single ensemble member for each model (hereafter referred to as the CMIP6 ensemble). This comparison aims to verify that the five SMILEs are representative of the full CMIP6 ensemble. This aforementioned comparison is performed using the historical and SSP5-8.5 scenarios.

2.2. Climate Indices

2.2.1. The Summer Rainfall Index

The Summer Rainfall Index (SRI) is computed following (Dieppois et al., 2016). For each grid point, we map the months of the monthly precipitation peak. SRI is defined as the region where precipitation peaks between December and February (Figure S1 in Supporting Information S1; blue contours in Figure 1b).

#### 2.2.2. Sea Surface Temperature and Atmospheric Circulation

We assess several drivers of precipitation variability based on both the results of Section 3 and the literature. We summarize these below:

- We assess the effect of ENSO, which has strong effects on southern African precipitation, by computing the Nino3.4 index [5°S–5°N; 190°–240°E] using Sea Surface Temperature (SST) anomalies following Barnston et al. (1999). The effect of the changes in Pacific SST on the large-scale atmospheric circulation is assessed by averaging the anomalies in 200 hPa velocity potential over the Pacific [20°S–20°N; 120°E−270°E], hereafter referred to as VP200.
- The variability of the Indian Ocean SSTs affects the southern African precipitation, and we use two different indices. We averaged the SST of the Indian Ocean [20°S–10°N; 60°E−120°E], and used the SIOD index, which is the difference between the western [37°S–27°S; 55°E−65°E] and eastern [28°S–18°S; 90°E−100°E] Indian Ocean SST (Behera & Yamagata, 2001).
- Desbiolles et al. (2020) show that the Angola-Benguela Frontal Zone (ABFZ) plays a key role in modulating the AL activity, hence impacting precipitation. The ABFZ index is calculated as the average of the SST over the eastern Southern Atlantic Ocean [21°S–9°S; 5°E−20°E].
- Pascale et al. (2019) show that changes in the upper-level atmospheric circulation affect southern African precipitation through the propagation of a Rossby Wave. We address the effect of changes in the upper-level tropospheric atmospheric circulation by averaging 200 hPa geopotential height anomalies (Z200) over the Southern Indian Ocean [60°S–20°S; 20°E−60°E].
- Variations in the location and strength of the AL affect precipitation over Southern Africa (Crétat et al., 2019; Munday & Washington, 2017; Pascale et al., 2019). We extract the location of the AL as the minimum of the 700 hPa relative vorticity over southern Africa, following Crétat et al. (2019). The meridional location of the AL is then defined as the latitudinal location of the minimum of the 700 hPa relative vorticity over southern Africa [25°S–8°S; 10°E−30°E] after performing a cubic spline interpolation, following Shekhar and Boos (2017).

2.2.3. Internal Variability and Externally Forced Response

Each ensemble member of a climate model provides an estimate of the change in precipitation that is due to both the effects of the externally forced response and internal climate variability. The latter is expected to be out of
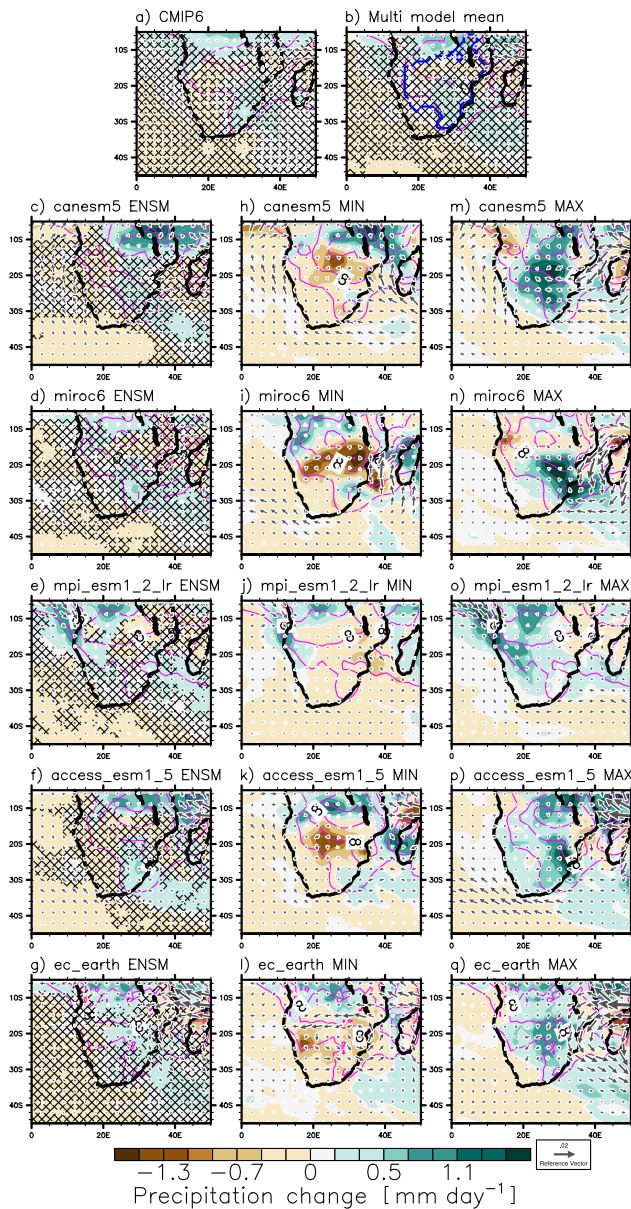
Figure 1. Near-term (2020–2040) change in DJF precipitation [colors; mm day^{-1}], for (a) the CMIP6 multi-model ensemble mean, (b) the multi-model mean of the 5 Single Model Initial-condition Large Ensembles (SMILEs) and for (c, g) each model, under the SSP5-8.5 emission scenario. Panels (h–q) show the ensemble mean of the two individual ensemble members that show the lowest (highest) change in Summer Rainfall Index (SRI) precipitation. Vectors show the change in surface moisture flux [kg kg^{-1} m s^{-1}]. The contours show the precipitation climatology (1995–2014), for each ensemble mean. On panels (a–o), the stippling indicates non-robust changes, that is, when 75% of the ensemble members/models disagree on the sign of the change compared to the ensemble mean. On panel (b), stippling indicates non-robust changes, that is, when at least 4 out of the 5 SMILEs do not agree with the sign of change, and the blue contour indicates SRI region.

phase between simulations. One assumption is that the ensemble mean of a large ensemble of simulations allows the difference between ensemble members to be removed, preserving the common part of the signal, which we assume to be the externally forced response. The externally forced response to climate is then defined as the ensemble mean of each SMILE. Following Deser et al. (2014), the effect of internal variability is then defined as the deviation from the externally forced response, as follows:

$$IV_{mv} = \Delta_{mv} - \overline{\Delta_v}, \tag{1}$$

where Δ denotes the change (future minus historical period) of a variable v, and for an ensemble member m. The overbar denotes an ensemble mean. IV_{mv} is the internal variability component and $\overline{\Delta_v}$ is the effect of climate change on each variable.

We follow the 6th Assessment Report of the Intergovernmental Panel on Climate Change (Chen et al., 2020) and define the effect of climate change over three different time horizons. We quantify near-term (2020–2040), mid-term (2040–2060) and long-term (2080–2100) changes in precipitation relative to the period 1995–2014. We assess changes in the core of the Austral summer season, that is, from December to February (DJF).

2.2.4. Highlighting the Effect of Internal Climate Variability

We assess the effects of internal climate variability on uncertainty in SRI changes by selecting the three ensemble members that show the strongest (i.e., stronger increase) and lowest (e.g., stronger decrease) changes in the internal component of SRI (following Equation 1), relative to the period 1995–2014. The selection is done for each year from 2015 to 2100 for each SMILE and each emissions scenario. This selection of ensemble members allows for the generation of a database containing a large number of events (i.e., two sets of 5,160 events: 5 SMILEs × 86 years × 3 ensemble members × 4 emissions scenarios). We merge all data together, assuming that the intra-SMILE ensemble variance is not dramatically impacted by the choice of the emissions scenario, as shown in Figure S2 in Supporting Information S1. This database is then used to assess the effects of internal climate variability on SRI change and detect its main drivers.

We assess the covariability of the drivers selecting ensemble members that simulate a strong evolution of the internal component of one of the selected drivers. We use the database that was previously defined and that is based on a selection of the ensemble members that show the extreme changes in SRI. For example, for the Z200-EN34 correlation, we selected ensemble members that simulate the strongest (negative and positive) changes in Z200 before calculating the correlation across these ensemble members between changes in Z200 and EN34. Note that we repeated the analysis the other way around, by selecting selected ensemble members that simulate the largest changes in EN34 before calculating the correlations but find only small changes in the coefficient correlation values.

2.3. Uncertainty in Precipitation Change

We assess uncertainty in precipitation change following Hawkins and Sutton (2011). We define three sources of uncertainty defined as the divergence between models, ensemble members and scenarios, using the four SMILEs:

1. **Model uncertainty** represents the difference between climate models in simulating future changes in precipitation. We first defined the effect of the externally forced response for each model and scenario (i.e., the multi-model mean). We then calculated the variance across all models for each scenario before calculating the average of the results across all scenarios.
2. The **scenario uncertainty** represents the difference between emissions scenarios in future changes in precipitation. We first calculated the ensemble mean across all models and ensemble members for each scenario before calculating the variance of the results across scenarios.
3. The **internal variability uncertainty** is the difference between the ensemble members of a single climate model. It is obtained by first calculating the variance across all ensemble members of each climate model and for each scenario before calculating the ensemble mean of the results across scenarios and models.
4. **Total uncertainty** is obtained as the sum of the model uncertainty, scenario uncertainty and internal variability uncertainty.

The obtained time series are finally smoothed by fitting a fourth-order polynomial, following Hawkins and Sutton (2011).

2.4. A Tale of Two Futures

We assess how and why different projections from the same model might diverge in simulating changes in southern African precipitation due to the effects of internal climate variability. We use the internal component (Equation 1) of the drivers of southern African precipitation variability (Section 2.2.3) and the database as obtained following Section 2.2.4. We perform a linear multiple regression to define how precipitation could change only because of the effects of the two main drivers of uncertainty identified in Section 3.2, such as:

$$IV.\text{SRI} = \alpha + \beta\,(IV.D1) + \gamma\,(IV.D2) + \epsilon \qquad (2)$$

where $IV.\text{SRI}$, $IV.D1$ and $IV.D2$ are the internal components of the SRI anomaly and the anomalies of the two selected drivers D1 and D2. α is the precipitation anomaly that is not due to the two drivers D1 and D2, β is the effect of D1 on precipitation, γ is the effect of D2 on precipitation. ϵ is the residual. α, β and γ are defined with multiple linear regression. We choose two drivers that can be defined as independent of each other, that is, with low co-variability.

3. Results

3.1. Externally Forced Response and Internal Climate Variability

The CMIP6 multi-model mean (Figure 1a) shows similar changes to the five SMILEs (Figure 1b) for the near-term horizon (2020–2040), with moderate precipitation change and a low inter-model agreement. The five SMILEs are thus representative of the entire CMIP6 ensemble, in terms of the pattern of the projected mean precipitation changes over southern Africa. The SMILEs ensemble also captures reasonably well the ensemble spread of the CMIP6 ensemble (not shown). Despite a change in magnitude, the same conclusion holds for the long-term change in precipitation (Figure S3 in Supporting Information S1).

The sign of precipitation change is only robust (i.e., 75% of agreement between ensemble members) over tropical and south-eastern southern Africa within most SMILEs (Figures 1c–1g). This inter-member disagreement is due to antagonistic changes between the ensemble members, with some projecting drier conditions and some others projecting wetter conditions (Figures 1h–1q). This large range of responses shows that the effect of internal climate variability is stronger than the externally forced response for the near-term horizon. Future changes in precipitation could, therefore, consist of either an increase or a decrease in precipitation over the period 2020–2040, following different sequences or pathways of internal climate variability. These different sequences of internal climate variability are associated with changes in the atmospheric dynamics, with an increase (a decrease) in southern African precipitation associated with northerly (southerly) wind anomaly at 850 hPa over the Mozambique Channel (Figure 1).

The effect of internal variability becomes weaker than the externally forced response in most of southern Africa in the long-term horizon (i.e., 2080–2100). This is particularly true over the areas covered by the South Indian Convergence Zone (eastern South Africa, southern Mozambique, and the southwestern Indian Ocean), where
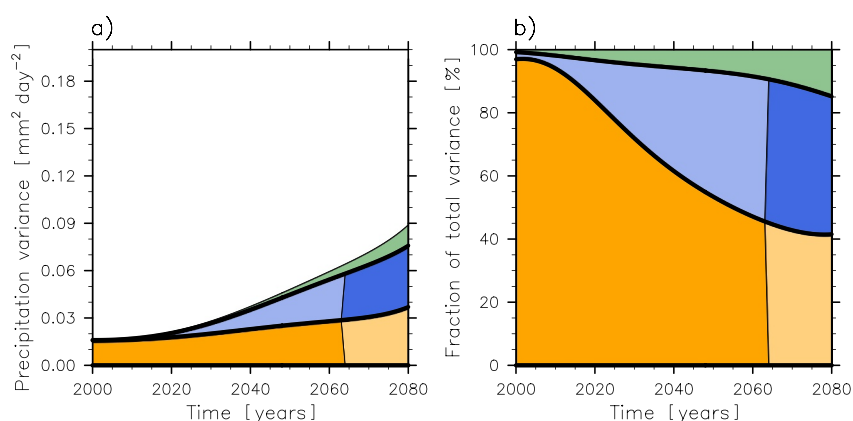
Figure 2. (a) Value of uncertainty and (b) fraction of total uncertainty in the Summer Rainfall Index (SRI) changes explained by each source of uncertainty. The internal variability is shown in orange, the model uncertainty in blue, and the scenario uncertainty in green. We applied a 20-year running mean to the SRI time series to smooth out noise. Dark (light) colors indicate which source of uncertainty contributes the most to the total uncertainty, that is, internal climate variability up to the 2050s and model uncertainty afterward.

most ensemble members show wetter conditions (Figure S3 in Supporting Information S1). However, the effect of internal climate variability remains high and the effect of the externally forced response remains highly model-sensitive, especially in the tropical-subtropical transition region.

We further confirm the results of Figure 1 by quantifying the effects of the three sources of uncertainty (internal climate variability, model, and scenario) in SRI change. All sources of uncertainty increase with time toward the end of the 21st century (Figure 2a). The strongest source of uncertainty for near-term and mid-term changes (2040–2060) in SRI relates to internal climate variability (Figure 2b). Model uncertainty and internal climate variability have a comparable weight in the total uncertainty for long-term changes in SRI (after 2080; Figure 2b). The internal climate variability uncertainty is thus the main source of uncertainty in SRI changes over the period 2000–2080. Unlike internal climate variability and model uncertainty, scenario uncertainty contributes only moderately to the total uncertainty in SRI change in the 21st century.

3.2. The Effect of Internal Climate Variability

Here, we aim to understand better the effect of internal climate variability on southern African precipitation, highlighting the mechanisms at play. We selected ensemble members (See Section 2.4) to pinpoint the mechanisms explaining the divergence induced by internal climate variability. In the following analysis, we compare the two sets of ensemble members by subtracting the one in which we have the decrease in SRI from the one in which we have the strongest increase in SRI. The selection of ensemble members is based on the change in SRI (see Section 2.4) and is therefore the same for each variable.

The effect of internal climate variability reveals a tripole in precipitation anomaly, with an increase in precipitation over southern Africa and a decrease in precipitation over Angola, the Congo Basin and Madagascar (Figure 3a). The increase in SRI is associated with a strengthening of the low-level wind over the Mozambique Channel, and south of Madagascar, which advect moisture from the tropical Indian Ocean. The change in low-level wind also allow advecting moisture from the Congo Basin. It is also associated with a strengthening and a southward shift of the AL (Figure 3b), and a decrease in Z850 (and SLP; not shown) over Botswana, Zambia and Zimbabwe, allowing the strengthening of the northerlies over the Mozambique Channel and the cyclonic circulation over land (Figure 3c). This pattern promotes inter-oceanic moisture convergence over southern Africa, by increasing moisture transport from the Indian Ocean basin and limiting moisture export over Angola toward the South Atlantic. (Figure 3a). Figure 3b also shows an increase in relative vorticity over the Mozambique Channel, which may indicate an awakened Mozambique Channel trough, which also contributes to shaping the precipitation anomaly pattern (Figure 3a), as shown in Barimalala et al. (2018). Figure 3 thus shows that there is a large inter-model agreement, with an increase in precipitation over southern Africa, a southward shift of the Angola Low and a strengthening of the low-level atmospheric circulation. In addition, Figure S5 in Supporting
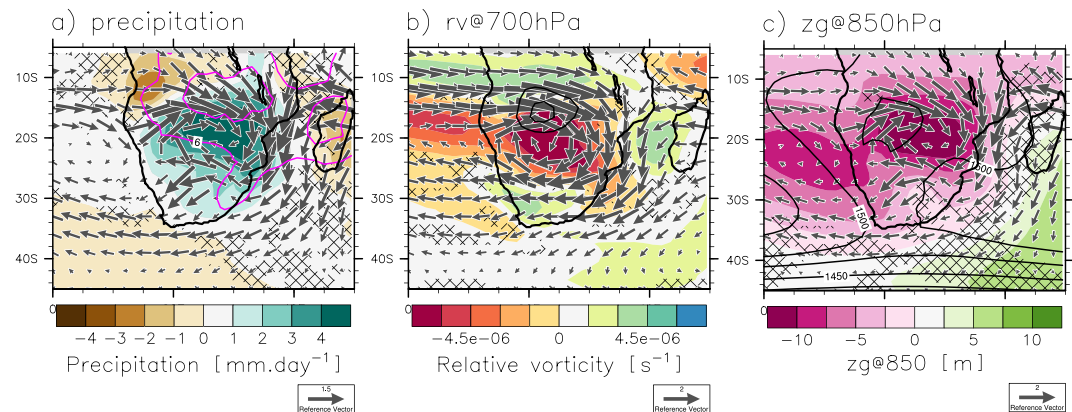
Figure 3. Effect of internal climate variability on changes in panel (a) precipitation [mm day^{-1}] and 850 hPa wind speed [m s^{-1}], (b) 700 hPa relative vorticity [s^{-1}] and wind speed [m s^{-1}], (c) Z850 [m] and 850 hPa wind speed [m s^{-1}]. The effect of internal climate variability is assessed as the difference between the ensemble members that show the more positive and more negative changes in Summer Rainfall Index (SRI), for each year over the period 2015–2100, selecting the internal component of all variables (see Section 2.2.3), and using data of all Single Model Initial-condition Large Ensembles (following Section 2.2.4). Stippling indicates that less than 4 models (out of 5) simulate an anomaly that is significant, according to a Student's *t* test at the 95% confidence level. The contours indicate a climatology that is defined by averaging together the events for which SRI change is the lowest (or more negative).

Information S1 shows remarkable similarities between the SMILEs concerning the effect of internal climate variability on precipitation and atmospheric circulation anomalies over southern Africa and the surrounding areas. The aforementioned results are consistent with the literature documenting interannual changes in southern African precipitation (e.g., Crétat et al., 2019; Dieppois et al., 2016, 2019; Pascale et al., 2019).

Anomalies in southern African precipitation are associated with changes in SST over the Pacific Ocean (e.g., Dieppois et al., 2016, 2019), the Indian Ocean (e.g., Behera & Yamagata, 2001), and the southeast Atlantic Ocean (e.g., Desbiolles et al., 2020). An increase in southern African precipitation is associated with a cooling of the tropical Indian Ocean, a La-Nina-like pattern and/or a negative IPV-like pattern in the tropical Pacific and a positive phase of the SIOD (Figure 4a; Dieppois et al., 2016). Sea Surface Temperature increases over the southwestern Indian Ocean and decreases over the north-eastern Indian Ocean, in a positive SIOD anomaly, which is known to favor moisture advection from the Indian Ocean into southern Africa (Behera & Yamagata, 2001). In addition, the increase in precipitation was associated with an increase in the SST of the Angola-Benguela front over the western South Atlantic Ocean (Figure 4a), affecting the AL (Desbiolles et al., 2020). There is a good inter-model agreement in SST anomalies over the Indian and Pacific Oceans (Figure 4a and Figure S6 in Supporting Information S1), although there are differences between the SMILEs on the pattern and magnitude of the SST anomaly over the equatorial and tropical Pacific Ocean (Figure S6 in Supporting Information S1).

Changes in SST influence and interact with the upper tropospheric circulation. Figure 4b shows that ENSO-induced strengthening of the Walker circulation promotes upper tropospheric divergence over southern Africa during La Nina events, hence increased precipitation there, in line with Dieppois et al. (2016) and Monerie et al. (2019). A warming of the western tropical Pacific Ocean (Figure 4a) could also contribute to the large-scale change in atmospheric circulation, promoting upper-level divergence (Figure 4b).

Another notable effect of internal climate variability is the alternation of negative and positive Z200 anomalies along the Austral Ocean, South America, and South Africa (Figure 4c). These anomalies indicate the presence of extratropical waves that can favor precipitation (Ivanciu et al., 2022; Ndarana et al., 2022, 2023), through their effects on the AL (Pascale et al., 2019).

In summary, there is generally a good agreement between the SMILEs regarding changes in SST and atmospheric circulation (Figure 4; Figure S6 in Supporting Information S1). We build on the existing literature and show that the modes of variability that influence the interannual variability of southern African precipitation can mask the effect of the externally forced response over the region and over a wide range of timescales. We also show that
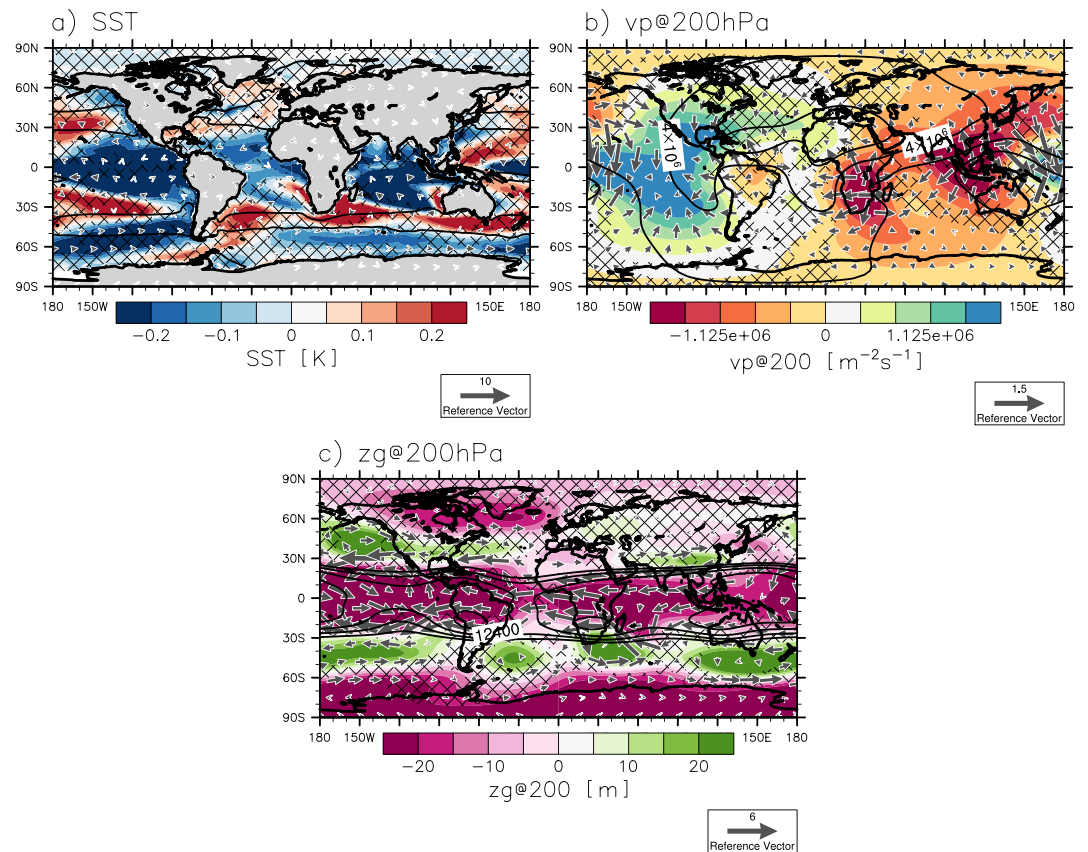
Figure 4. As in Figure 3 but for (a) Sea Surface Temperature [K] and 850 hPa wind speed [m s^{-1}], (b) 200 hPa velocity potential [m^{-2} s^{-1}] and divergent wind speed [s^{-1}], and (c) 200 hPa geopotential height [m] and wind speed [m s^{-1}].

results also hold when using periods of 20 years (Figure S4 in Supporting Information S1). However, we show that the SMILEs overestimate precipitation and 700 hPa relative vorticity over southern Africa (Figure S7 in Supporting Information S1), potentially leading to an overestimated uncertainty in precipitation change. We assume that this scientific question would require an in-depth analysis of the representation of the Angola Low and its relationship with precipitation variability in climate models (see, for instance, Munday & Washington, 2017).

3.3. Drivers of Uncertainty in Changes in Southern African Precipitation

Possible drivers of uncertainty in southern African precipitation change were identified in the previous section. However, we have not quantified the relative role of the linkages between each plausible ocean-atmosphere driver of future changes in southern African rainfall. We also did not identify a priori the main source of uncertainty for future changes in SRI. Here, we assess the role of each driver of uncertainty in southern African precipitation by calculating the correlation coefficient between the change in SRI and each plausible ocean-atmosphere driver. This is achieved by selecting ensemble members that show the strongest and lowest changes in SRI for each year, scenario, and model (5,160 events, see Section 2.2.4).

The two main drivers of uncertainty are identified to be the changes in 200 hPa velocity potential (VP200; $r = 0.45$ between changes in VP200 and SRI) over the equatorial Pacific Ocean and the meridional location of the AL ($r = 0.69$ between changes in the meridional location of the AL and SRI) (Figure 5a). Both drivers of future precipitation changes are independent, with a low and non-significant correlation coefficient calculated between the change in AL and VP200 ($r = -0.13$). Thus, a large change in the meridional position of AL can occur with no change in VP200 over the equatorial Pacific and vice versa. This is consistent with Pascale et al. (2019), Howard and Washington (2018), Reason and Jagadheesha 2005, who show that the interannual variability in the AL location is not due to changes in ENSO and, hence, of the resulting VP200 anomalies. The SIOD (Indian Ocean
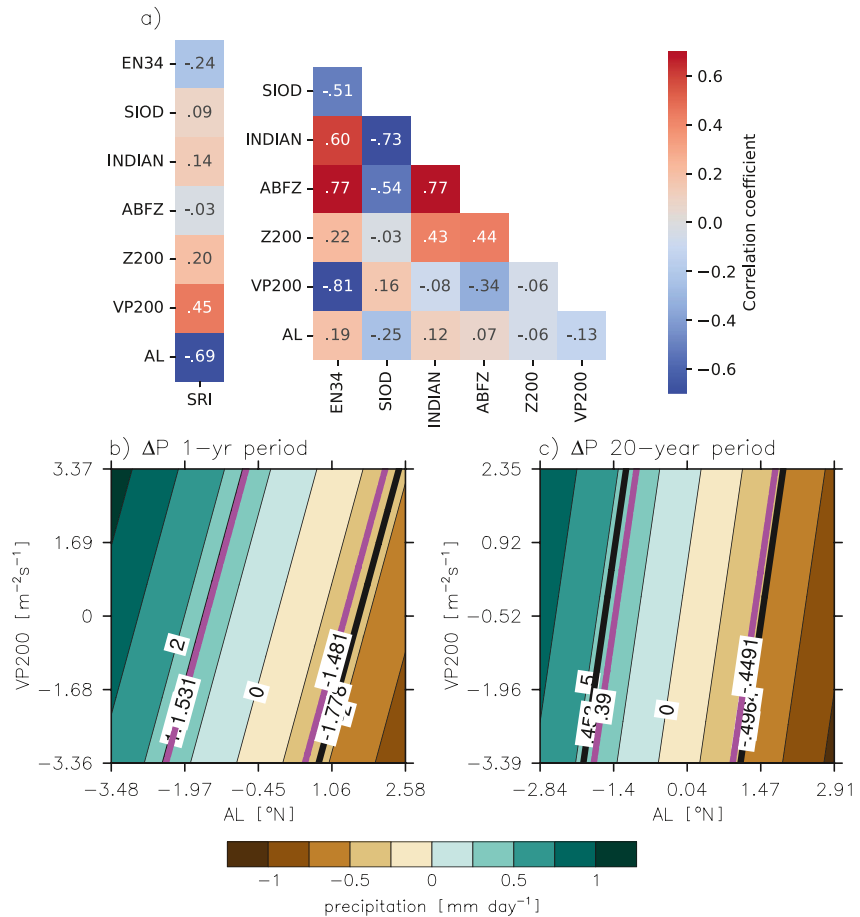
Figure 5. (a) (left) Correlation coefficient computed between the changes in Summer Rainfall Index (SRI) and in several drivers of SRI variability (defined in Section 2), and (right) between drivers. The correlation between drivers and SRI is calculated by selecting ensemble members (Section 2.2.4). Prediction of the SRI anomaly depending on the future change in AL meridional location and 200 hPa velocity potential over the equatorial Pacific Ocean, selecting SRI anomalies of each (b) individual year and (c) the three 20-year time horizons (near-, mid-, and long-term changes), in a storyline approach, following Section 2. The purple lines show the extreme predicted changes, and the black lines show the actual extreme changes in SRI (10th and 90th percentiles of the distribution).

SSTs) and Z200 also explain the uncertainty in SRI change but have a weaker impact than the meridional location of the AL and VP200 ($r = 0.09$ between changes in SIOD and SRI and $r = 0.20$ between changes in Z200 and SRI). We expect the change in VP200 to be driven primarily by changes in equatorial Pacific SST but find a weaker relationship between the change in EN34 and SRI ($r = -0.24$ between changes in EN34 and SRI). We suggest that this weak relationship between changes in EN34 and SRI is due to differences between models in simulating changes in the eastern tropical Pacific and its relationship to southern African rainfall (Figure 4a). This could be a focus for further study.

Here we provide a projection of plausible future different trajectories of SRI change as a function of changes in the meridional location of the AL and of the VP200 index, following Equation 2, without accounting for the residual. Differences between trajectories then only depend on different future changes in the AL meridional location and equatorial Pacific VP200 anomalies. The correlation coefficient between the projected change in SRI and the actual change in SRI is $r = 0.80$, showing that this statistical model can explain 64% of the uncertainty in SRI change. This means that almost two-thirds of the uncertainty in SRI change is due to the uncertainty in the change in the AL meridional location and equatorial Pacific VP200 anomalies.

The future change in SRI is shown in Figure 5b, using the range of outcomes in AL meridional location and VP200 as obtained across all ensemble members of all SMILEs, assessing both the effects of internal climate

variability and the externally forced response. A northward shift of the AL and a decrease in the equatorial Pacific VP200 lead to a decrease in SRI, while a southward shift of the AL and a strengthening of VP200 is associated with an increase in SRI (Figure 5b). The aforementioned discussed relationships between the AL, VP200 and precipitation are consistent with Crétat et al. (2019), Pascale et al. (2019), and Howard and Washington (2018). Figure 5b shows that the main driver in SRI uncertainty is the meridional location of the AL, which leads to either a decrease or an increase in SRI. Meanwhile, VP200 anomalies have a weaker influence and only moderately modulate regional precipitation. To highlight the dominant role of the AL, we have reproduced our analysis but using a linear regression (only one driver) and selecting the AL as a unique driver, we then explain ∼60% of the uncertainty with the AL alone. We find that the AL is the main source of uncertainty for southern African precipitation change, a result that is consistent with Munday and Washington (2017), which show that the difference between models in simulating the AL is the main source of uncertainty for simulating historical variations in southern African precipitation.

We also assess how this framework could represent the extreme variations in SRI precipitation. First, we show the extreme changes in precipitation by calculating the 10% and 90% percentiles in SRI change (black lines in Figure 5b). We also show the extreme predicted changes in SRI (black lines in Figure 5b). The statistical model can reproduce both the overall change in SRI, as well as the extreme changes in SRI. This conclusion also holds when changes averaged over 20-year periods are assessed (Figure 5c), highlighting that changes in the meridional location of the AL and the equatorial Pacific VP200 can affect projections of southern African precipitation from interannual to multi-decadal timescales. We can then conclude that a better understanding of future changes in AL activity, as well as equatorial Pacific VP200 anomalies (and thus ENSO and Pacific SST changes in general), is needed.

In addition to the statistical model, we show how changes in AL meridional location and VP200 anomalies can modulate SRI for a given emissions scenario. For each year, we selected the three ensemble members that show the larger northward/southward shift of the Angolan low and the stronger 200 hPa wind convergence/divergence over the equatorial Pacific and show their projected change in SRI (Figure 6). The ensemble spread is greater than the effect of climate change over the 20th and 21st centuries (Figures 6a–6f), in agreement with Figure 1. We show that the effect of the uncertainty in the location of the meridional location of the AL is greater than the effect of the uncertainty in VP200. The effect of an uncertain AL location largely explains the ensemble spread in SRI change, for the multi-model mean (Figure 6a) and for each model (Figures 6b–6f). Figure 6 shows that the respective effects of each driver of uncertainty are model-dependent and that they vary with time.

The strong effect of uncertainty in the location of the AL on changes in SRI, for each model, is consistent with the fact that the uncertainty in its location is mainly due to internal climate variability (Figure 6g). By contrast, model uncertainty is strong for VP200, particularly by the end of the 21st century (Figure 6h).

4. Discussion

Future changes in precipitation are uncertain because of divergences in the processes that allow atmospheric convection to occur (e.g., moisture flux convergence, temperature anomalies and changes in radiative forcing), and because of differences between climate models in simulating atmospheric convection (e.g., differences in atmospheric convection schemes and microphysics, in horizontal and vertical resolution). Uncertainty also arises from uncertainty in simulating the regional and large-scale climate drivers of precipitation. We show that the uncertainty in the simulation of future changes in southern African precipitation is strongly tied to the simulation of the effects of internal climate variability on southern African climate, through changes in the meridional location of the AL and the large-scale Walker circulation. However, we do not argue that the uncertainty in simulating changes in southern African precipitation can be explained solely by changes in the AL and the Walker circulation. First, we show that other drivers may be of importance for the changes in southern African precipitation, such as the change in Rossby waves activity over the Austral Ocean (Figure 3). Second, we show that, although there are strong similarities between the results of the different SMILEs, large-scale drivers of precipitation changes may be model-dependent. Meanwhile, the Walker circulation anomaly is weaker in ACCESS-ESM1-5 than in the other models (Figure S6 in Supporting Information S1). Similarly, the pattern of the Z200 anomalies differs between SMILEs over the Austral Ocean, being more homogeneous in ACCESS-ESM1-5 than in MIROC6 (Figure S6 in Supporting Information S1). A major driver of precipitation changes could, therefore, be the Southern Annular Mode in ACCESS-ESM1-5 (as in Gillett et al. (2006)) and the propagation of a Rossby
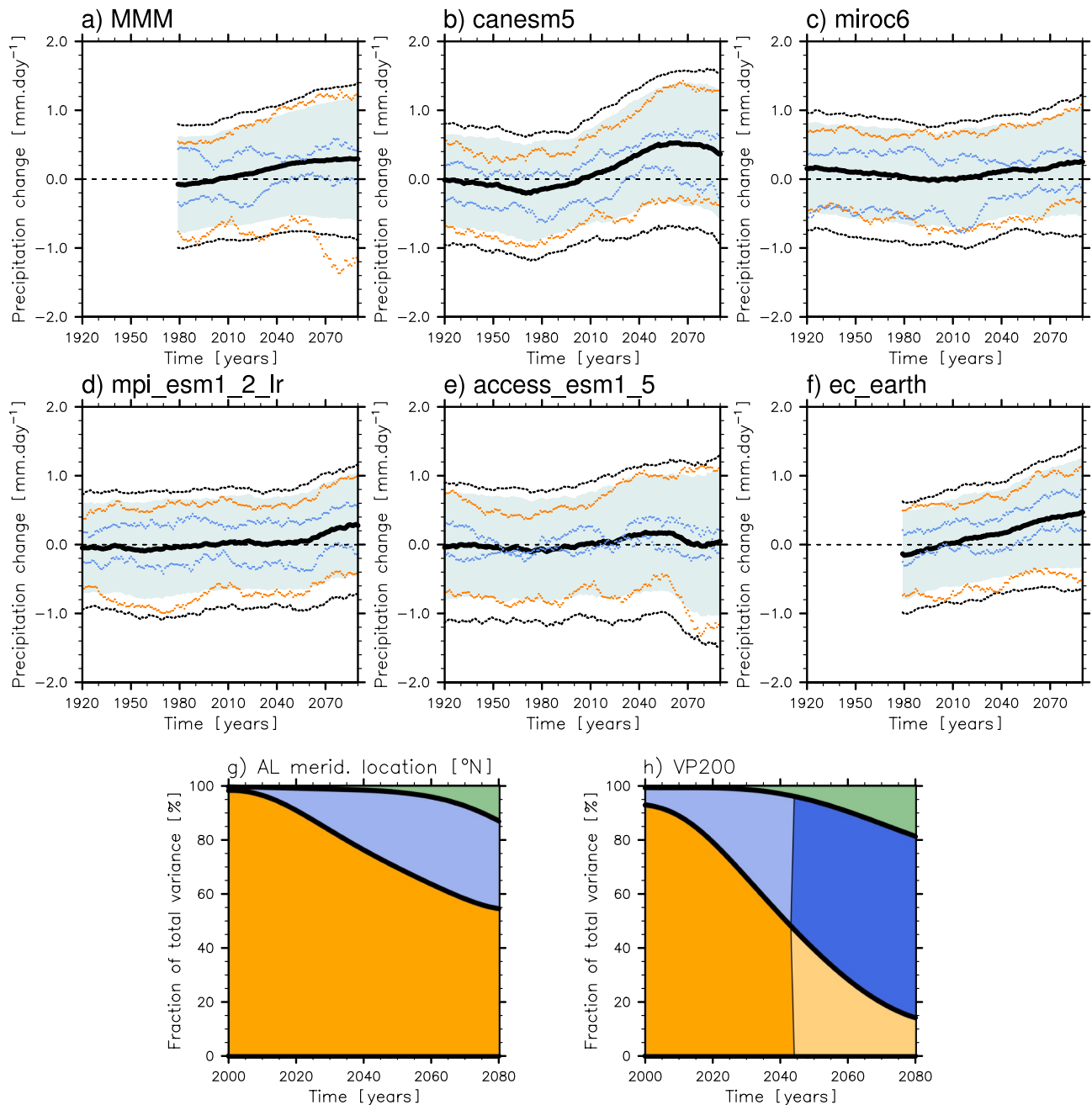
Figure 6. Time series of Summer Rainfall Index change (relative to the period 1995–2014) for the ensemble mean (thick black line), the ensemble spread (blue shading; the ensemble standard deviation), the 10th and 90th percentiles (thin dashed black line), and that due to the uncertainty in the simulation of the meridional location of the Angola low (orange dots) and the 200 hPa wind convergence over the eastern tropical Pacific (blue dots). Results are given for (a) the ensemble of all models and ensemble members, and for (b–f) each Single Model Initial-condition Large Ensemble. The time series have been smoothed with a 20-year running mean. (g, h), as in Figure 2b, but for the meridional location of the Angola low and VP200.

Wave in MIROC6 (as in Pascale et al. (2019)). A more in-depth analysis may be required to understand the cause of the uncertainty in each SMILE. Finally, we do not assess changes in soil moisture and land surface feedback, which were discarded as a main driver of southern African climate variability by Pascale et al. (2019).

Other sources of uncertainty may be related to differences between climate models in simulating changes in the interhemispheric temperature gradient (Munday & Washington, 2019). Here, we find no evidence for the role of

the large-scale interhemispheric temperature gradient (Figure 4a), which is mostly associated with the effect of the externally forced response rather than internal climate variability.

In contrast to the literature, we do not show a strong correlation between the change in the AL activity and the ABFZ SSTs (in Desbiolles et al. (2020)) and the Z200 anomaly (as in Pascale et al. (2019)). The aforementioned hiatus could be due to the horizontal resolution of SMILEs, which is relatively coarse compared to the data sets used in Desbiolles et al. (2020) and Pascale et al. (2019), climate models biases, or because the patterns of South Atlantic SST and Z200 changes are model dependent. We do not rule out the possibility that the eastern South Atlantic SST or anomalies in the extratropical Z200 play a role in the changes in southern African precipitation and its uncertainty. Similarly, we do not show a major effect of an uncertain simulation of the SIOD on southern African precipitation. This is not consistent with Hoell et al. (2017) and Hoell and Cheng (2018). However, we do not rule out the possibility of SIOD affecting southern African rainfall (as seen in Figure 4a for instance). We replicated the analysis of Section 3.3 using the EN3.4 and SIOD indices but found that it only explains ~20% of the uncertainty in future precipitation changes. These results are, however, model-dependent. For instance, we found that the Indian Ocean temperature is a strong source of uncertainty in the simulation of southern African precipitation in MPI-ESM1-2-LR (not shown), and we also hypothesize that the dominance of the AL could be due to higher uncertainty in the simulation of the future change of the AL than the other drivers.

We show that the meridional position of the Angola Low is the main source of uncertainty for the future change in SRI. We also tested the effect of an uncertain change in the strength of the Angola Low. There is no robust relationship between the change in the meridional location of the Angola Low and its strength (not shown) and the statistical model run with solely the strength of the Angola Low only explains ~2% of the uncertainty in the SRI change.

We argue that a better understanding of the above sources of uncertainty could improve the simulation of future changes in southern African precipitation. A consequence of the uncertainty in the SRI change is that the SMILEs show a robust time of emergence (i.e., when the externally forced response is stronger than the effect of internal climate variability) only at a few locations (Figure S8 in Supporting Information S1).

5. Conclusion

We assess future changes in precipitation over southern Africa using five SMILEs forced by four emissions scenarios. We show that the effect of the externally forced response is weak due to model uncertainty and internal variability uncertainty. The latter obscures the effect of externally forced changes and leads to either a decrease or an increase in southern African precipitation. The internal climate variability uncertainty is found to be the main source of uncertainty for the 21st century. Understanding the drivers of uncertainty in future southern African precipitation change is critical for anticipating future problems caused by for example, multi-year droughts, hence threatening water and food security, as well as hydroelectric production.

We show that future projected changes in southern African precipitation depend mainly on the future change in the meridional location of the Angola Low (AL). We show that ~60% of the uncertainty in the change in southern African precipitation is due to the uncertainty in simulating the change in the meridional location of the AL. This is consistent with Munday and Washington (2017) who show that the simulation of the AL is the main source of bias for southern African precipitation in general circulation models. This is also consistent with Howard and Washington (2020) which show uncertainty in future change in frequency and shift in tropical lows to correlate with the inter model spread in southern African precipitation change among CMIP5 models.

Besides the AL, we show that uncertainty in simulating the change in the Walker circulation (a decrease in atmospheric vertical rise over the western Pacific due to a cooling of its equatorial part) also explains a non-negligible proportion of the uncertainty. Both the equatorial Pacific Sea Surface Temperature (SST) and the location of the AL are known drivers of southern African precipitation variability and are relatively independent (e.g., Crétat et al., 2019; Dieppois et al., 2016, 2019, 2015; Howard et al., 2019; Howard & Washington, 2018; Pascale et al., 2019). Thus, we show that future changes in southern African precipitation will strongly depend on the future evolution of the Angola Low and the large-scale Walker circulation. We acknowledge that understanding better the future change of these aforementioned drivers of southern African precipitation could allow for improving the projections of the southern African precipitation change, as also argued by Dieppois et al. (2021) for the Pacific Ocean SST characteristics. We show that these two drivers affect both the short-term

(the year to come) to the longer-term (for 20 years) evolution of southern African precipitation over the 21st century.

Previous studies have shown that climate change is associated with an increase in precipitation and temperature variability globally (Rehfeld et al., 2020; Thornton et al., 2014). A future increase in the variability of the AL meridional location and large-scale Walker circulation strength could lead to a stronger uncertainty in projections of the southern African precipitation. This could be the topic of further study. Another follow-up would be to apply an emergent constraint approach to the Angola Low's meridional location to reduce uncertainty in projections of southern African precipitation. We also suggest here that calibrating the general circulation models (e.g., O'Reilly et al., 2021, 2020) using the interannual variability of the Angola Low location may allow the improvement of southern African precipitation projections, but this would require a better understanding of the reasons for the variability of the Angola Low and its effect on precipitation. Besides, a combination of decadal forecasts and uninitialized simulations may also be used to reduce uncertainty over the first part of the 21st century (e.g., Befort et al., 2022) allowing the development of a seamless prediction of the southern African precipitation. Another follow-up of the study would be to assess drivers of southern African precipitation change for each individual month and for a different season.

Data Availability Statement

CMIP6 GCM output is available from public repositories, including https://esgf-index1.ceda.ac.uk/search/cmip6-ceda/.

References

Almazroui, M., Saeed, F., Saeed, S., Nazrul Islam, M., Ismail, M., Klutse, N. A. B., & Siddiqui, M. H. (2020). Projected change in temperature and precipitation over Africa from CMIP6. *Earth Systems and Environment*, *4*(3), 455–475. https://doi.org/10.1007/s41748-020-00161-x

Ayugi, B., Eresanya, E. O., Onyango, A. O., Ogou, F. K., Okoro, E. C., Okoye, C. O., et al. (2022). Review of meteorological drought in Africa: Historical trends, impacts, mitigation measures, and prospects. *Pure and Applied Geophysics*, *179*(4), 1365–1386. https://doi.org/10.1007/s00024-022-02988-z

Barimalala, R., Desbiolles, F., Blamey, R. C., & Reason, C. (2018). Madagascar influence on the Southsouth Indian Ocean convergence zone, the Mozambique channel trough and Southern African rainfall. *Geophysical Research Letters*, *45*(20), 11–311. https://doi.org/10.1029/2018GL079964

Barnston, A. G., He, Y., & Glantz, M. H. (1999). Predictive skill of statistical and dynamical climate models in SST forecasts during the 1997—98 El Niño episode and the 1998 La Niña onset. *Bulletin of the American Meteorological Society*, *80*(2), 217–243. https://doi.org/10.1175/1520-0477(1999)080<0217:PSOSAD>2.0.CO;2

Befort, D. J., Brunner, L., Borchert, L. F., O'Reilly, C. H., Mignot, J., Ballinger, A. P., et al. (2022). Combination of decadal predictions and climate projections in time: Challenges and potential solutions. *Geophysical Research Letters*, *49*(15), e2022GL098568. https://doi.org/10.1029/2022GL098568

Behera, S. K., & Yamagata, T. (2001). Subtropical SST dipole events in the Southern Indian Ocean. *Geophysical Research Letters*, *28*(2), 327–330. https://doi.org/10.1029/2000GL011451

Burls, N. J., Blamey, R. C., Cash, B. A., Swenson, E. T., Fahad, A. A., Bopape, M.-J. M., et al. (2019). The cape town "Day zero" drought and Hadley cell expansion. *Npj Climate and Atmospheric Science*, *2*(1), 27. https://doi.org/10.1038/s41612-019-0084-6

Chen, Z., Zhou, T., Zhang, L., Chen, X., Zhang, W., & Jiang, J. (2020). Global land monsoon precipitation changes in CMIP6 projections. *Geophysical Research Letters*, *47*(14), e2019GL086902. https://doi.org/10.1029/2019GL086902

Conway, D., Dalin, C., Landman, W. A., & Osborn, T. J. (2017). Hydropower plans in eastern and southern Africa increase risk of concurrent climate-related electricity supply disruption. *Nature Energy*, *2*(12), 946–953. https://doi.org/10.1038/s41560-017-0037-4

Crétat, J., Pohl, B., Dieppois, B., Berthou, S., & Pergaud, J. (2019). The Angola low: Relationship with southern African rainfall and ENSO. *Climate Dynamics*, *52*(3), 1783–1803. https://doi.org/10.1007/s00382-018-4222-3

Crétat, J., Richard, Y., Pohl, B., Rouault, M., Reason, C., & Fauchereau, N. (2012). Recurrent daily rainfall patterns over South Africa and associated dynamics during the core of the austral summer. *International Journal of Climatology*, *32*(2), 261–273. https://doi.org/10.1002/joc.2266

Dallas, H. F., & Rivers-Moore, N. (2014). Ecological consequences of global climate change for freshwater ecosystems in South Africa. *South African Journal of Science*, *110*(5/6), 1–11. https://doi.org/10.1590/sajs.2014/20130274

Desbiolles, F., Howard, E., Blamey, R. C., Barimalala, R., Hart, N. C. G., & Reason, C. J. C. (2020). Role of ocean mesoscale structures in shaping the Angola-low pressure system and the southern Africa rainfall. *Climate Dynamics*, *54*(7), 3685–3704. https://doi.org/10.1007/s00382-020-05199-1

Deser, C., Phillips, A. S., Alexander, M. A., & Smoliak, B. V. (2014). Projecting North American climate over the next 50 Years: Uncertainty due to internal variability. *Journal of Climate*, *27*(6), 2271–2296. https://doi.org/10.1175/JCLI-D-13-00451.1

Dieppois, B., Capotondi, A., Pohl, B., Chun, K. P., Monerie, P.-A., & Eden, J. (2021). ENSO diversity shows robust decadal variations that must be captured for accurate future projections. *Communications Earth & Environment*, *2*(1), 212. https://doi.org/10.1038/s43247-021-00285-6

Dieppois, B., Pohl, B., Crétat, J., Eden, J., Sidibe, M., New, M., et al. (2019). Southern African summer-rainfall variability, and its teleconnections, on interannual to interdecadal timescales in CMIP5 models. *Climate Dynamics*, *53*(5), 3505–3527. https://doi.org/10.1007/s00382-019-04720-5

Dieppois, B., Pohl, B., Rouault, M., New, M., Lawler, D., & Keenlyside, N. (2016). Interannual to interdecadal variability of winter and summer southern African rainfall, and their teleconnections. *Journal of Geophysical Research: Atmospheres*, *121*(11), 6215–6239. https://doi.org/10.1002/2015JD024576

Dieppois, B., Rouault, M., & New, M. (2015). The impact of ENSO on Southern African rainfall in CMIP5 ocean atmosphere coupled climate models. *Climate Dynamics*, *45*(9), 2425–2442. https://doi.org/10.1007/s00382-015-2480-x

Dosio, A., Jury, M. W., Almazroui, M., Ashfaq, M., Diallo, I., Engelbrecht, F. A., et al. (2021). Projected future daily characteristics of African precipitation based on global (CMIP5, CMIP6) and regional (CORDEX, CORDEX-CORE) climate models. *Climate Dynamics*, *57*(11), 3135–3158. https://doi.org/10.1007/s00382-021-05859-w

Eyring, V., Bony, S., Meehl, G. A., Senior, C. A., Stevens, B., Stouffer, R. J., & Taylor, K. E. (2016). Overview of the Coupled Model Inter-comparison Project Phase 6 (CMIP6) experimental design and organization. *Geoscientific Model Development*, *9*(5), 1937–1958. https://doi.org/10.5194/gmd-9-1937-2016

Gaughan, A. E., Staub, C. G., Hoell, A., Weaver, A., & Waylen, P. R. (2016). Inter- and Intra-annual precipitation variability and associated relationships to ENSO and the IOD in southern Africa. *International Journal of Climatology*, *36*(4), 1643–1656. https://doi.org/10.1002/joc.4448

Gillett, N. P., Kell, T. D., & Jones, P. D. (2006). Regional climate impacts of the southern annular mode. *Geophysical Research Letters*, *33*(23). https://doi.org/10.1029/2006GL027721

Gore, M., Abiodun, B. J., & Kucharski, F. (2020). Understanding the influence of ENSO patterns on drought over southern Africa using SPEEDY. *Climate Dynamics*, *54*(1), 307–327. https://doi.org/10.1007/s00382-019-05002-w

Hawkins, E., & Sutton, R. (2011). The potential to narrow uncertainty in projections of regional precipitation change. *Climate Dynamics*, *37*, 407–418.

Hoell, A., & Cheng, L. (2018). Austral summer Southern Africa precipitation extremes forced by the El Ni{ñ}o-Southern oscillation and the subtropical Indian Ocean dipole. *Climate Dynamics*, *50*(9), 3219–3236. https://doi.org/10.1007/s00382-017-3801-z

Hoell, A., Gaughan, A. E., Shukla, S., & Magadzire, T. (2017). The hydrologic effects of synchronous El Niño–Southern Oscillation and sub-tropical Indian Ocean Dipole events over southern Africa. *Journal of Hydrometeorology*, *18*(9), 2407–2424. https://doi.org/10.1175/JHM-D-16-0294.1

Howard, E., & Washington, R. (2018). Characterizing the synoptic expression of the Angola low. *Journal of Climate*, *31*(17), 7147–7165. https://doi.org/10.1175/JCLI-D-18-0017.1

Howard, E., & Washington, R. (2020). Tracing future spring and summer drying in southern Africa to tropical lows and the Congo air boundary. *Journal of Climate*, *33*(14), 6205–6228. https://doi.org/10.1175/JCLI-D-19-0755.1

Howard, E., Washington, R., & Hodges, K. I. (2019). Tropical lows in southern Africa: Tracks, rainfall contributions, and the role of ENSO. *Journal of Geophysical Research: Atmospheres*, *124*(21), 11009–11032. https://doi.org/10.1029/2019JD030803

Ivanciu, I., Ndarana, T., Matthes, K., & Wahl, S. (2022). On the ridging of the South Atlantic anticyclone over South Africa: The impact of Rossby wave breaking and of climate change. *Geophysical Research Letters*, *49*(20), e2022GL099607. https://doi.org/10.1029/2022GL099607

Lehner, F., Deser, C., Maher, N., Marotzke, J., Fischer, E. M., Brunner, L., et al. (2020). Partitioning climate projection uncertainty with multiple large ensembles and CMIP5/6. *Earth System Dynamics*, *11*(2), 491–508. https://doi.org/10.5194/esd-11-491-2020

Li, C., Chai, Y., Yang, L., & Li, H. (2016). Spatio-temporal distribution of flood disasters and analysis of influencing factors in Africa. *Natural Hazards*, *82*(1), 721–731. https://doi.org/10.1007/s11069-016-2181-8

Maher, N., Milinski, S., Suarez-Gutierrez, L., Botzet, M., Dobrynin, M., Kornblueh, L., et al. (2019). The max Planck institute grand ensemble: Enabling the exploration of climate system variability. *Journal of Advances in Modeling Earth Systems*, *11*(7), 2050–2069. https://doi.org/10.1029/2019MS001639

Malherbe, J., Dieppois, B., Maluleke, P., Van Staden, M., & Pillay, D. L. (2016). South African droughts and decadal variability. *Natural Hazards*, *80*(1), 657–681. https://doi.org/10.1007/s11069-015-1989-y

Malherbe, J., Landman, W. A., & Engelbrecht, F. A. (2014). The bi-decadal rainfall cycle, southern annular mode and tropical cyclones over the Limpopo River Basin, southern Africa. *Climate Dynamics*, *42*(11), 3121–3138. https://doi.org/10.1007/s00382-013-2027-y

Mauritsen, T., Bader, J., Becker, T., Behrens, J., Bittner, M., Brokopf, R., et al. (2019). Developments in the MPI-M Earth system model version 1.2 (MPI-ESM1.2) and its response to increasing CO_2. *Journal of Advances in Modeling Earth Systems*, *11*(4), 998–1038. https://doi.org/10.1029/2018MS001400

Monerie, P.-A., Robson, J., Dong, B., Dieppois, B., Pohl, B., & Dunstone, N. (2019). Predicting the seasonal evolution of southern African summer precipitation in the DePreSys3 prediction system. *Climate Dynamics*, *52*(11), 6491–6510. https://doi.org/10.1007/s00382-018-4526-3

Monerie, P.-A., Sanchez-Gomez, E., Pohl, B., Robson, J., & Dong, B. (2017). Impact of internal variability on projections of Sahel precipitation change. *Environmental Research Letters*, *12*(11), 114003. https://doi.org/10.1088/1748-9326/aa8cda

Munday, C., & Washington, R. (2017). Circulation controls on southern African precipitation in coupled models: The role of the Angola Low. *Journal of Geophysical Research: Atmospheres*, *122*(2), 861–877. https://doi.org/10.1002/2016JD025736

Munday, C., & Washington, R. (2019). Controls on the diversity in climate model projections of early summer drying over southern Africa. *Journal of Climate*, *32*(12), 3707–3725. https://doi.org/10.1175/JCLI-D-18-0463.1

Ndarana, T., Lekoloane, L. E., Rammopo, T. S., Reason, C. J. C., Bopape, M.-J. M., Chikoore, H., & Engelbrecht, F. A. (2023). Downstream development during ridging South Atlantic Ocean anticyclones. *Climate Dynamics*, *61*(5), 2865–2883. https://doi.org/10.1007/s00382-023-06717-7

Ndarana, T., Rammopo, T. S., Reason, C. J. C., Bopape, M.-J., Engelbrecht, F., & Chikoore, H. (2022). Two types of ridging South Atlantic Ocean anticyclones over South Africa and the associated dynamical processes. *Atmospheric Research*, *265*, 105897. https://doi.org/10.1016/j.atmosres.2021.105897

O'Reilly, C. H., Befort, D. J., & Weisheimer, A. (2020). Calibrating large-ensemble European climate projections using observational data. *Earth System Dynamics*, *11*(4), 1033–1049. https://doi.org/10.5194/esd-11-1033-2020

O'Reilly, C. H., Befort, D. J., Weisheimer, A., Woollings, T., Ballinger, A., & Hegerl, G. (2021). Projections of Northern Hemisphere extra-tropical climate underestimate internal variability and associated uncertainty. *Communications Earth & Environment*, *2*(1), 194. https://doi.org/10.1038/s43247-021-00268-7

Pascale, S., Kapnick, S. B., Delworth, T. L., & Cooke, W. F. (2020). Increasing risk of another cape town "Day Zero" drought in the 21st century. *Proceedings of the National Academy of Sciences*, *117*(47), 29495–29503. https://doi.org/10.1073/pnas.2009144117

Pascale, S., Pohl, B., Kapnick, S. B., & Zhang, H. (2019). On the Angola low interannual variability and its role in modulating ENSO effects in Southern Africa. *Journal of Climate*, *32*(15), 4783–4803. https://doi.org/10.1175/JCLI-D-18-0745.1

Pohl, B., Dieppois, B., Crétat, J., Lawler, D., & Rouault, M. (2018). From synoptic to interdecadal variability in southern African rainfall: Toward a unified view across time scales. *Journal of Climate*, *31*(15), 5845–5872. https://doi.org/10.1175/JCLI-D-17-0405.1

Pohl, B., Macron, C., & Monerie, P.-A. (2017). Fewer rainy days and more extreme rainfall by the end of the century in Southern Africa. *Scientific Reports*, *7*(1), 46466. https://doi.org/10.1038/srep46466

Ratna, S. B., Behera, S., Ratnam, J. V., Takahashi, K., & Yamagata, T. (2013). An index for tropical temperate troughs over southern Africa. *Climate Dynamics*, *41*(2), 421–441. https://doi.org/10.1007/s00382-012-1540-8

Ratnam, J. V., Behera, S. K., Masumoto, Y., & Yamagata, T. (2014). Remote effects of El Niño and modoki events on the austral summer precipitation of Southern Africa. *Journal of Climate*, *27*(10), 3802–3815. https://doi.org/10.1175/JCLI-D-13-00431.1

Reason, C. J. C., & Jagadheesha, D. (2005). A model investigation of recent ENSO impacts over southern Africa. *Meteorology and Atmospheric Physics*, *89*(1), 181–205. https://doi.org/10.1007/s00703-005-0128-9

Reason, C. J. C., Landman, W., & Tennant, W. (2006). Seasonal to decadal prediction of southern African climate and its links with variability of the Atlantic Ocean. *Bulletin of the American Meteorological Society*, *87*(7), 941–955. https://doi.org/10.1175/BAMS-87-7-941

Reason, C. J. C., & Rouault, M. (2002). ENSO-like decadal variability and South African rainfall. *Geophysical Research Letters*, *29*(13), 14–16. https://doi.org/10.1029/2002GL014663

Rehfeld, K., Hébert, R., Lora, J. M., Lofverstrom, M., & Brierley, C. M. (2020). Variability of surface climate in simulations of past and future. *Earth System Dynamics*, *11*(2), 447–468. https://doi.org/10.5194/esd-11-447-2020

Shekhar, R., & Boos, W. R. (2017). Weakening and shifting of the Saharan shallow meridional circulation during wet years of the West African Monsoon. *Journal of Climate*, *30*(18), 7399–7422. https://doi.org/10.1175/JCLI-D-16-0696.1

Siderius, C., Gannon, K. E., Ndiyoi, M., Opere, A., Batisani, N., Olago, D., et al. (2018). Hydrological response and complex impact pathways of the 2015/2016 El Niño in Eastern and Southern Africa. *Earth's Future*, *6*(1), 2–22. https://doi.org/10.1002/2017EF000680

Swart, N. C., Cole, J. N. S., Kharin, V. V., Lazare, M., Scinocca, J. F., Gillett, N. P., et al. (2019). The Canadian Earth System Model Version 5 (CanESM5.0.3). *Geoscientific Model Development*, *12*(11), 4823–4873. https://doi.org/10.5194/gmd-12-4823-2019

Tatebe, H., Ogura, T., Nitta, T., Komuro, Y., Ogochi, K., Takemura, T., et al. (2019). Description and basic evaluation of simulated mean state, internal variability, and climate sensitivity in MIROC6. *Geoscientific Model Development*, *12*(7), 2727–2765. https://doi.org/10.5194/gmd-12-2727-2019

Thornton, P. K., Ericksen, P. J., Herrero, M., & Challinor, A. J. (2014). Climate variability and vulnerability to climate change: A review. *Global Change Biology*, *20*(11), 3313–3328. https://doi.org/10.1111/gcb.12581

Tramblay, Y., Villarini, G., Saidi, M. E., Massari, C., & Stein, L. (2022). Classification of flood-generating processes in Africa. *Scientific Reports*, *12*(1), 18920. https://doi.org/10.1038/s41598-022-23725-5

Ukkola, A. M., De Kauwe, M. G., Roderick, M. L., Abramowitz, G., & Pitman, A. J. (2020). Robust future changes in meteorological drought in CMIP6 projections despite uncertainty in precipitation. *Geophysical Research Letters*, *47*(11), e2020GL087820. https://doi.org/10.1029/2020GL087820

Ullah, A., Pohl, B., Pergaud, J., Dieppois, B., & Rouault, M. (2023). Intraseasonal descriptors and extremes in South African rainfall. Part II: Summer teleconnections across multiple timescales. *International Journal of Climatology*, *43*(8), 3799–3827. https://doi.org/10.1002/joc.8059

Wolski, P., Conradie, S., Jack, C., & Tadross, M. (2021). Spatio-temporal patterns of rainfall trends and the 2015–2017 drought over the winter rainfall region of South Africa. *International Journal of Climatology*, *41*(S1), E1303–E1319. https://doi.org/10.1002/joc.6768

Wu, Y., Miao, C., Slater, L., Fan, X., Chai, Y., & Sorooshian, S. (2024). Hydrological projections under CMIP5 and CMIP6: Sources and magnitudes of uncertainty. *Bulletin of the American Meteorological Society*, *105*(1), E59–E74. https://doi.org/10.1175/BAMS-D-23-0104.1

Wyser, K., van Noije, T., Yang, S., von Hardenberg, J., O'Donnell, D., & Döscher, R. (2020). On the increased climate sensitivity in the EC-Earth model from CMIP5 to CMIP6. *Geoscientific Model Development*, *13*(8), 3465–3474. https://doi.org/10.5194/gmd-13-3465-2020

Ziehn, T., Chamberlain, M. A., Law, R. M., Lenton, A., Bodman, R. W., Dix, M., et al. (2020). The Australian Earth System Model: ACCESS-ESM1.5. *Journal of Southern Hemisphere Earth Systems Science*, *70*(1), 193–214. https://doi.org/10.1071/ES19035

References From the Supporting Information

Adler, R. F., Huffman, G. J., Chang, A., Ferraro, R., Xie, P.-P., Janowiak, J., et al. (2003). The version-2 Global Precipitation Climatology Project (GPCP) monthly precipitation analysis (1979–present). *Journal of Hydrometeorology*, *4*(6), 1147–1167. https://doi.org/10.1175/1525-7541(2003)004<1147:TVGPCP>2.0.CO;2

Boucher, O., Servonnat, J., Albright, A. L., Aumont, O., Balkanski, Y., Bastrikov, V., et al. (2020). Presentation and evaluation of the IPSL-CM6A-LR climate model. *Journal of Advances in Modeling Earth Systems*, *12*(7), e2019MS002010. https://doi.org/10.1029/2019MS002010

Cao, J., Wang, B., Yang, Y.-M., Ma, L., Li, J., Sun, B., et al. (2018). The Nuist Earth System Model∼(NESM) version 3: Description and preliminary evaluation. *Geoscientific Model Development*, *11*(7), 2975–2993. https://doi.org/10.5194/gmd-11-2975-2018

Cherchi, A., Fogli, P. G., Lovato, T., Peano, D., Iovino, D., Gualdi, S., et al. (2019). Global mean climate and main patterns of variability in the CMCC-CM2 coupled model [JOUR]. *Journal of Advances in Modeling Earth Systems*, *11*(1), 185–209. https://doi.org/10.1029/2018MS001369

Danabasoglu, G., Lamarque, J.-F., Bacmeister, J., Bailey, D. A., DuVivier, A. K., Edwards, J., et al. (2020). The Community Earth System Model Version 2 (CESM2). *Journal of Advances in Modeling Earth Systems*, *12*(2), e2019MS001916. https://doi.org/10.1029/2019MS001916

Delworth, T., Stouffer, R., Dixon, K., Spelman, M., Knutson, T., Broccoli, A., et al. (2002). Review of simulations of climate variability and change with the GFDL R30 coupled climate model. *Climate Dynamics*, *19*(7), 555–574. https://doi.org/10.1007/s00382-002-0249-5

Dong, X., Jin, J., Liu, H., Zhang, H., Zhang, M., Lin, P., et al. (2021). CAS-ESM2.0 model datasets for the CMIP6 ocean model Intercomparison Project Phase 1 (OMIP1). *Advances in Atmospheric Sciences*, *38*(2), 307–316. https://doi.org/10.1007/s00376-020-0150-3

Dunne, J. P., Horowitz, L. W., Adcroft, A. J., Ginoux, P., Held, I. M., John, J. G., et al. (2020). The GFDL Earth System Model Version 4.1 (GFDL-ESM 4.1): Overall coupled model description and simulation characteristics. *Journal of Advances in Modeling Earth Systems*, *12*(11), e2019MS002015. https://doi.org/10.1029/2019MS002015

Golaz, J.-C., Caldwell, P. M., Van Roekel, L. P., Petersen, M. R., Tang, Q., Wolfe, J. D., et al. (2019). The DOE E3SM coupled model version 1: Overview and evaluation at standard resolution. *Journal of Advances in Modeling Earth Systems*, *11*(7), 2089–2129. https://doi.org/10.1029/2018MS001603

Held, I. M., Guo, H., Adcroft, A., Dunne, J. P., Horowitz, L. W., Krasting, J., et al. (2019). Structure and performance of GFDL's CM4.0 climate model. *Journal of Advances in Modeling Earth Systems*, *11*(11), 3691–3727. https://doi.org/10.1029/2019MS001829

Kanamitsu, M., Ebisuzaki, W., Woollen, J., Yang, S.-K., Hnilo, J. J., Fiorino, M., et al. (2002). NCEP–DOE AMIP-II reanalysis (R-2). *Bulletin of the American Meteorological Society*, *83*(11), 1631–1643. https://doi.org/10.1175/BAMS-83-11-1631

Kelley, M., Schmidt, G. A., Nazarenko, L. S., Bauer, S. E., Ruedy, R., Russell, G. L., et al. (2020). GISS-E2.1: Configurations and climatology. *Journal of Advances in Modeling Earth Systems*, *12*(8), e2019MS002025. https://doi.org/10.1029/2019MS002025

Kuhlbrodt, T., Jones, C. G., Sellar, A., Storkey, D., Blockley, E., Stringer, M., et al. (2018). The low-resolution version of HadGEM3 GC3.1: Development and evaluation for global climate. *Journal of Advances in Modeling Earth Systems*, *10*(11), 2865–2888. https://doi.org/10.1029/2018MS001370

Lee, J., Kim, J., Sun, M.-A., Kim, B.-H., Moon, H., Sung, H. M., et al. (2020). Evaluation of the Korea meteorological administration advanced community earth-system model (K-ace). *Asia-Pacific Journal of Atmospheric Sciences*, *56*(3), 381–395. https://doi.org/10.1007/s13143-019-00144-7

Lee, W.-L., Wang, Y.-C., Shiu, C.-J., Tsai, I., Tu, C.-Y., Lan, Y.-Y., et al. (2020). Taiwan Earth system model version 1: Description and evaluation of mean state. *Geoscientific Model Development*, *13*(9), 3887–3904. https://doi.org/10.5194/gmd-13-3887-2020

Li, J., Bao, Q., Liu, Y., Wu, G., Wang, L., He, B., et al. (2019). Evaluation of FAMIL2 in simulating the climatology and seasonal-to-interannual variability of tropical cyclone characteristics. *Journal of Advances in Modeling Earth Systems*, *11*(4), 1117–1136. https://doi.org/10.1029/2018MS001506

Li, L., Yu, Y., Tang, Y., Lin, P., Xie, J., Song, M., et al. (2020). The flexible global ocean-atmosphere-land system model grid-point version 3 (FGOALS-g3): Description and evaluation. *Journal of Advances in Modeling Earth Systems*, *12*(9), e2019MS002012. https://doi.org/10.1029/2019MS002012

Lin, Y., Huang, X., Liang, Y., Qin, Y., Xu, S., Huang, W., et al. (2020). Community Integrated Earth System Model (CIESM): Description and evaluation. *Journal of Advances in Modeling Earth Systems*, *12*(8), e2019MS002036. https://doi.org/10.1029/2019MS002036

Lovato, T., Peano, D., Butenschön, M., Materia, S., Iovino, D., Scoccimarro, E., et al. (2022). CMIP6 simulations with the CMCC Earth system model (CMCC-ESM2). *Journal of Advances in Modeling Earth Systems*, *14*(3), e2021MS002814. https://doi.org/10.1029/2021MS002814

Mulcahy, J. P., Johnson, C., Jones, C. G., Povey, A. C., Scott, C. E., Sellar, A., et al. (2020). Description and evaluation of aerosol in UKESM1 and HadGEM3-GC3.1 CMIP6 historical simulations. *Geoscientific Model Development*, *13*(12), 6383–6423. https://doi.org/10.5194/gmd-13-6383-2020

Müller, W. A., Jungclaus, J. H., Mauritsen, T., Baehr, J., Bittner, M., Budich, R., et al. (2018). A higher-resolution version of the max planck institute Earth system model (MPI-ESM1.2-HR). *Journal of Advances in Modeling Earth Systems*, *10*(7), 1383–1413. https://doi.org/10.1029/2017MS001217

Rong, X., Li, J., Chen, H., Su, J., Hua, L., Zhang, Z., & Xin, Y. (2021). The CMIP6 historical simulation datasets produced by the climate system model CAMS-CSM. *Advances in Atmospheric Sciences*, *38*(2), 285–295. https://doi.org/10.1007/s00376-020-0171-y

Séférian, R., Nabat, P., Michou, M., Saint-Martin, D., Voldoire, A., Colin, J., et al. (2019). Evaluation of CNRM Earth system model, CNRM-ESM2-1: Role of Earth system processes in present-day and future climate. *Journal of Advances in Modeling Earth Systems*, *11*(12), 4182–4227. https://doi.org/10.1029/2019MS001791

Seland, Ø., Bentsen, M., Olivié, D., Toniazzo, T., Gjermundsen, A., Graff, L. S., et al. (2020). Overview of the Norwegian Earth System Model (NorESM2) and key climate response of CMIP6 DECK, historical, and scenario simulations. *Geoscientific Model Development*, *13*(12), 6165–6200. https://doi.org/10.5194/gmd-13-6165-2020

Semmler, T., Danilov, S., Gierz, P., Goessling, H. F., Hegewald, J., Hinrichs, C., et al. (2020). Simulations for CMIP6 with the AWI climate model AWI-CM-1-1. *Journal of Advances in Modeling Earth Systems*, *12*(9), e2019MS002009. https://doi.org/10.1029/2019MS002009

Shi, X., Chen, X., Dai, Y., & Hu, G. (2020). Climate sensitivity and feedbacks of BCC-CSM to idealized CO_2 forcing from CMIP5 to CMIP6. *Journal of Meteorological Research*, *34*(4), 865–878. https://doi.org/10.1007/s13351-020-9204-9

Swapna, P., Krishnan, R., Sandeep, N., Prajeesh, A. G., Ayantika, D. C., Manmeet, S., & Vellore, R. (2018). Long-term climate simulations using the IITM Earth system model (IITM-ESMv2) with focus on the South Asian Monsoon. *Journal of Advances in Modeling Earth Systems*, *10*(5), 1127–1149. https://doi.org/10.1029/2017MS001262

Voldoire, A., Saint-Martin, D., Sénési, S., Decharme, B., Alias, A., Chevallier, M., et al. (2019). Evaluation of CMIP6 DECK experiments with CNRM-CM6-1. *Journal of Advances in Modeling Earth Systems*, *11*(7), 2177–2213. https://doi.org/10.1029/2019MS001683

Volodin, E. M., Mortikov, E. V., Kostrykin, S. V., Galin, V. Y., Lykossov, V. N., Gritsun, A. S., et al. (2017). Simulation of the present-day climate with the climate model INMCM5. *Climate Dynamics*, *49*(11), 3715–3734. https://doi.org/10.1007/s00382-017-3539-7

Volodin, E. M., Mortikov, E. V., Kostrykin, S. V., Galin, V. Y., Lykossov, V. N., Gritsun, A. S., et al. (2018). Simulation of the modern climate using the INM-CM48 climate model. *Russian Journal of Numerical Analysis and Mathematical Modelling*, *33*(6), 367–374. https://doi.org/10.1515/rnam-2018-0032

Yukimoto, S., Kawai, H., Koshiro, T., Oshima, N., Yoshida, K., Urakawa, S., et al. (2019). The meteorological Research institute Earth system model version 2.0, MRI-ESM2.0: Description and basic evaluation of the physical component. *Journal of the Meteorological Society of Japan. Ser. II*, *97*(5), 931–965. https://doi.org/10.2151/jmsj.2019-051